Improvement of Dielectric Properties of Natural Rubber by Adding Perovskite Nanoparticles

Neudys González[1,2], Maria del Àngels Custal[2], Said Lalaouna[2], Jordi-Roger Riba[3*], Elaine Armelin[1,4*]

[1]*Departament d'Enginyeria Química, Universitat Politècnica de Catalunya, Av. Diagonal 647, 08028, Barcelona, Spain.*

[2]*Sicame Company, C/ Zinc, 14 – Polígono Industrial Aquiberia, 08755, Castellbisbal, Barcelona, Spain.*

[3]*Departament d'Enginyeria Elèctrica, Universitat Politècnica de Catalunya, C. Colom, 1, 08222, Terrassa, Spain.*

[4]*Center for Research in Nano-Engineering, Universitat Politècnica de Catalunya, Campus Sud, Edifici C', C/Pasqual i Vila s/n, 08028, Barcelona, Spain.*

Correspondence to: elaine.armelin@upc.edu and riba@ee.upc.edu

ABSTRACT

Natural rubber matrix, reinforced with several conventional stabilizer additives, was further charged with perovskite nanoparticles. Although the addition of $BaTiO_3$ ceramic particles usually transforms a non-conducting pristine polymer into a more conductive polymer composite, in this case we use the addition of a few percent of $BaTiO_3$ (less than 1 wt.%) to decrease the effective electrical conductivity of natural rubber (NR). This reduction has been attributed to the synergistic effect between ceramic particles and the amorphous phase of the polymer matrix, which allowed decreasing ~~of~~ the interfacial polarization among the NR/oxide particles interfaces. Electrical tests clearly indicate that the breakdown voltage increases and the leakage current decreases, whereas the mechanical and hydrophobicity properties of solid films??? improve after accurate sonication of all solid particles before pre-vulcanization process. Therefore, the dielectric elastomer becomes more insulating with the addition of nanometric oxide particles.

Keywords: Natural rubber, perovskite, nanocomposites, dielectric breakdown, permittivity.

1. INTRODUCTION

Nowadays, natural rubber (NR) remains attractive for several applications due to its low-temperature flexibility, high elasticity, fatigue resistance, tearing resistance, low heat buildup and building tack. NR is important in the production of thin-walled products such as surgical gloves, ballons, tires, or as suspension element in buildings, to resist earthquakes, and bridges, to accommodate bridge deck movements. However, natural rubber materials technology, *i.e.* the technology of making rubber parts from natural rubber, requires extensive compounding. A typical recipe contains elastomeric polymer, filler, plasticizer, antidegradants, processing or flow agent, vulcanizing agent, vulcanization accelerator and activators, and so on. Therefore, the properties of the final product depend very strongly on the specific compound formulation [1] and processing [2].

Nanotechnology offers wonderful products to approach nanoscale dimensions for compounding. Nanoparticles, nanorods, nanowires, nanospheres, nanofibers, are most of the current terms being employed for different types ~~forms~~ of nanoscale materials. The advantage to use nanomaterials for compounding is ~~a result of~~ the dramatic change of ~~in~~ physicochemical ~~physical chemistry~~ properties, which can also depend ~~be dependent~~ on their anisotropy [3]. Independently from their nanoscale form, the key for obtaining excellent and reproducible properties is the good dispersion inside the polymer matrix. Improvement of solid and insoluble particles dispersion mixtures has been achieved with ball-milling techniques [4] or high-frequency sound vibrations transmitted by ultrasonic equipment to homogenize and disrupt agglomerates when ceramic molecules are employed, among others [5]. Furthermore, the surface chemical modification of inorganic micro- and nanoparticles has also been developed as another strategy to avoid segregation during their incorporation in hydrophobic polymer matrices [6-8]. The surface modifiers, bearing different functional groups, may enhance the matrix-filler compatibility thus reducing the polarity difference. Nevertheless, the latter solution is usually too expensive for real application in the manufacture of latex at industrial sector.

Therefore, the incorporation of inorganic nanoparticles into polymers has opened up novel opportunities to prepare the dielectric materials applied in embedded capacitors. In recent years, ~~In this way,~~ traditional ferroelectric ceramics (e.g. $BaTiO_3$, $PbTiO_3$, $LiNbO_3$, and others) have ~~been~~ attracted increasing interest because of their capability for withstanding

high electric field and energy densities when incorporated to isolating polymers [9]. They exhibit high dielectric constant and usually low dielectric strength. Currently, barium titanate is being extensively applied in photovoltaic devices to improve the energy efficiency in thin film transistors, solar cells, and other energy harvesting applications [10,11]. Meanwhile, isolating polymers have high breakdown strengths (4.50–8.50 MV/cm), low dielectric loss (tan δ) ~ 0.0002 and low dielectric permittivity (ε) ~ 2.5–5 at 1 kHz [12,13].

Much research has already been done and reported in the employment of barium titanate as filler in ~~to~~ insulating ~~isolating~~ polymers like epoxy [14-16], polyvinylidene fluoride [5,7,8], and also in natural rubber [4,17]. However, high filler loading (>10%) can complicate the processing of the material, thus decreasing ~~of~~ the mechanical properties and ~~also~~ leading to poor application in the NR industry.

Therefore, the introduction of micro/nanofillers into the NR matrix, with well dispersed particles and very low concentrations, is a good choice for property enhancement of NR technology.

In this work we developed a new composite with improved insulating properties after the incorporation of a very low concentration of ceramic dielectric molecules. Thus, the aim of the present work is to assess the synergistic effect obtained by the incorporation of $BaTiO_3$ nanoparticles (~100 nm) with TiO_2 and ZnO ceramic particles, inside the latex material. $BaTiO_3$ nanoparticles were chosen due to their high relative permittivity or dielectric constant (ε_r), which is three-six??? times higher than TiO_2. Thus, several properties like thermal stability, morphology, electrical conductivity and dielectric permittivity were explored. Additionally, by combining the low cost, ease of processing and high breakdown field strength of latex with the high permittivity of $BaTiO_3$ fillers will result in high-energy storage capability. Major research efforts have been focused towards developing high dielectric constant (ε), low dielectric loss (tanδ) and high electrical breakdown dielectrics for highly insulating natural rubber.

2. EXPERIMENTAL SECTION

2.1. Materials. NR latex was purchased from several suppliers and used as received. Barium titanate nanopowder ($BaTiO_3$, particle size <100 nm), zinc oxide (ZnO) and titanium dioxide

(TiO_2) were supplied by Sigma Aldrich Spain. Sulfur (reagent grade) and Zinc Dibuthyl dithiocarbamate (ZDBC) were used as vulcanizing agent and accelerator, respectively. Dispersant agents used for $BaTiO_3$ mixing were oleic acid (Sigma-Aldrich Spain) and Cab-o-Sperse® (Cabot Corporation). Fillers and other ingredients added to the latex formulation were of commercial grade.

2.2. Preparation of NR films modified with $BaTiO_3$ nanoparticles

NR/$BaTiO_3$ nanocomposites i $BaTiO_3$ loadings in the range 0-0.5 weight % were prepared at 23°C using a Heidolph mechanical overhead stirrer model (RZR-1) provided with radial flow impeller stirrer blade, with a rotor speed of 60 rpm. The compounding formulations used for the preparation of NR/$BaTiO_3$ nanocomposites are shown in Table 1. For solid barium titanate mixing, 500 mg $BaTiO_3$ nanoparticles were added to 3 ml of oleic acid ~~or~~ of dispersant agent Cab-o-Sperse®. Then the suspension was subjected to ultrasonic dispersion for 20 min using Sonopuls Ultrasonic Homogenizers (Bandelin, model HD 2200). This homogeneous distribution is a prerequisite for obtaining a uniform coating in the subsequent steps. Therefore, all solids were dispersed and sonicated before addition to the rubber emulsion. In a typical fabrication procedure, NR was first masticated for 5 min. Zinc oxide was added and mixed for 2 min and then mixed with stearic acid for 2 min. Barium titanate powder was finally added into the mixing chamber after the pre-dispersion explained before. After dumping the mixes out, ZDBC was added and mixed for 2 min, then sulfur similarly with 2 min mixing. The NR emulsion was then stirred for 30 min.

2.3. Preparation of NR films

The rubber compound was then sheeted out or poured onto glass substrate or tube test specimens which were dipped in the liquid suspension and left to pre-vulcanize at 76ºC for 3h in an oven for obtaining the solid film. Afterwards samples were washed gradually in a bath with distilled water from 25 to 70ºC, dried and then left to complete curing for 24 h before testing. The complete process to obtain the film can be seen in the Scheme 1.

2.4. Characterization. A Specac model MKII Golden Gate attenuated total reflection (ATR) with a heated Diamond ATR Top-Plate was used for the infrared spectroscopy analysis. Differential scanning calorimetry (DSC) was performed using a TA Instruments Q100 series equipped with a refrigerated cooling system (RCS) operating at temperatures from -90 ºC to

200 ºC. Experiments were conducted under a flow of dry nitrogen with a sample weight of approximately 5 mg and calibration was performed with indium. The glass transition temperatures (T_g) of the vulcanized samples were determined from the second heating curve after sample fast cooling to -90ºC. Thermogravimetric analysis (TGA) was carried out with a Q50 thermogravimetric analyzer of TA Instruments at a heating rate of 10 ºC/min under nitrogen atmosphere and a temperature range from 30 ºC to 600 ºC. Inspection of the cryo-fractured surfaces of NR films was conducted by scanning electron microscopy (SEM) using a Focus Ion Beam Zeiss Neon 40 instrument (Carl Zeiss, Germany). Conductive carbon coating was deposited on the film surface by using a Mitec K950 Sputter Coater before SEM analyses. Samples were visualized at an accelerating voltage of 5 kV and the EDX at 3kV. Diameter of all sonicated solid particles was measured with the SmartTiff software from Carl Zeiss SMT Ltd. Contact angle measurements were performed employing OCA 20 (DataPhysics Instruments GmbH, Filderstadt) equipment and using the droplet sessile method at room temperature. For the static contact angle (sCA) measurements, 1 μL droplets of distillated water were dispensed on the respective surfaces. Images of distilled water drops were recorded after drop stabilization (30 s). The contact angle values (software SCA 20) were obtained as the average of ten independent measures for each sample. Mechanical properties were evaluated with JBA Testing Machine model 853 and using dumbbell shaped specimen with 75 mm of length, 3 mm of width and 1.0 mm of thickness. Tensile testing was conducted at room temperature with a deformation rate of 500 mm/min and the mechanical parameters were averaged over a total of 5 measurements for each probe.

2.5. Electrical resistivity and dielectric relaxation properties

The surface and volume resistivity's of films were measured with an Agilent HP 16008A resistivity cell with a constant DC voltage of 500V for 1 min (followed by 5 min of discharge mode) or 5 min (followed by 30 min of discharge mode), according to the ASTM D257-07 standard [18]. The film thickness varied from 700 to 1000 μm, the diameter of disks was 12 cm and the relativity humidity was maintained below 70% RH for all measurements.

The dielectric response was measured using an impedance analyzer Autolab PGSTAT 302N in the frequency range from 10 mHz to 1MHz and the amplitude of the sinusoidal voltage was 10 mV. All experiments were carried at room temperature. Appropriated sized films

were cut in a disc format and were sandwiched between two stainless steel electrodes (diameter = 1.5 cm) assembled into an isolating resin holder [19]. The cell was tightened with screws to ensure constant fastening pressure. Films thickness was about 750 μm, determined by a micrometer, and the working area was 1.766 cm^2. Prior cell closing, samples were immersed in NaCl 3,5wt.% at room temperature for 24 hours and the water excess wiped out with a tissue. After data collection, EIS results were then processed and fitted to an electrical equivalent circuit (EEC). Relative permittivity was then calculated from capacitance, knowing the area and thickness of each sample.

The AC dielectric tests were carried out on insulating films by using the dielectric test setup described in the IEC-60903 standard. A Phenix BK130/36 high voltage dielectric test set equipped with precision calibrated digital metering to accomplish the requirements of the IEC-60903 and ASTM D120–09 standards [20] was used for this purpose. It allows raising the voltage applied to the test samples from 0 volt up to breakdown conditions and measuring simultaneously the leakage current and the applied voltage. Three samples of each formulation were measured to take into account the inherent variability. Since the thickness of the tested latex samples is slightly different, both leakage current and voltage were normalized to unity (1 mm) thickness.

3. RESULTS AND DISCUSSION

Characterization of perovskite nanoparticles

It is well know that the dielectric properties of composites strongly depend on the dispersion of different phases. Due to the high hydrophobicity of natural rubber, the incorporation of $BaTiO_3$ ceramic particles, mixed with solids and liquids additives used in the conventional ~~old-stablished~~ latex fabrication, is not an easy task. Latex resin usually coagulates under hard stirring processes and moreover, the morphology of $BaTiO_3$ is affected by the solvent and surfactant natures, and also by the pH value. It is expected that the incorporation of nano-sized $BaTiO_3$ powders would also help their dispersion in the latex suspension. However, to obtain thinner high-dielectric permittivity ceramic/polymer composite films, it is necessary to study the best way to add perovskite. Nowadays, there are several approaches being explored, such as surface functionalization [6], sol-gel [8], colloidal processing [21],

ball-milling or other physical mixing technique [4]. For example, Jiang and co-workers [9] functionalized barium titanate with thiol groups and ultra-small silver (Ag) nanoparticles for further incorporation to polyvinylidene fluoride (PVDF) matrix and they obtained improved electrical properties. Another example is the recent works reported by Li and co-workers [22,23]. They modified $BaTiO_3$ nanoparticles by using hydrogen peroxide and a salt oil derivative from oleic acid to improve the dispersion capability in organic solvents.

In this work, we ~~wanted~~ avoided ceramic functionalization and other exhaustive methods with the aim of simplifying the process for real application in ~~latex~~ industrial ~~processing~~ systems. Thus, in order to get the better dispersion option of $BaTiO_3$ particles before the incorporation to latex resin, to avoid particles aggregation, two simple approaches were considered using common additives employed in rubber preparation. Firstly, the nanoparticles were previously dispersed in an oil emulsion usually added in a very low concentration and moreover used to unmould the solid rubber from molds after vulcanization; and secondly, the nanoparticles were added to a dispersant agent usually employed to help solid mixing with the liquid resin.

It was observed by SEM that the first approach does not work just to the $BaTiO_3$ further aggregation inside the oil emulsion (Figure 1a-b), which was apparently well dispersed before addition. After the solid film formation, it resulted in visible agglomerates on the coating surface (Figure 1c). On the other hand, optimum dispersion conditions were obtained for suspensions prepared with the Cab-o-Sperse® dispersant agent, which is a neutral agent particularly indicated for water-based systems in a pH range from 3.5-10.5. Particle size was analysed by SEM before and after dispersion by ultrasonication and after solid film formation. Figure 2a shows barium titanate particles with nanometric size of 187 ± 49 nm before addition to the latex emulsion and Figure 2b shows the morphology surface of a well dispersed zinc, titanium and barium oxides inside the vulcanized rubber films (NR/$BaTiO_3$-0.50wt %). Presence of $BaTiO_3$ was localized in some areas indicated in Figure 2b, with the EDX composition shown in Figure 2c, and the particle sizes varied from 560 to 780 nm.

Characterization of NR/$BaTiO_3$ solid films with variable concentration of perovskite

Structural characterization of solid films was performed with infrared spectroscopy. Figure 3 shows a comparison between pristine NR and NR/$BaTiO_3$-0.50wt% composites. As can be seen, the main absorption bands from saturated aliphatic –C-H groups (2914cm^{-1}, 2848cm^{-1}, strectching; 1542cm^{-1}, 1461cm^{-1}, 1373cm^{-1}, bending bands; 723cm^{-1}, out-of-plane bending vibrations) appears accentuated in the film composite prepared after ultrasonication and with decreased particles size, whereas unsaturated =C-H has been decreased (2960cm^{-1}, stretching; 1648cm^{-1}, bending band). Therefore, it is due to the better dispersion achieved after sonication process and thus better radical polymerization reaction between *cis*-1,4 poli(isopreno) chains, *i.e.* perovskite particles have actuated as a cross-linker promoter. Additionally, the only one absorption band from ceramic additives found in the elastomers films is that from silicates (1012 cm^{-1}, Si-O-Si), which are usually strong. None absorption band from $BaTiO_3$ nanoparticles added to the latex formulation were observed due to the very low concentration and well mixing process.

Thermal characterization was performed with DSC and TGA analyses. The glass transition temperature is not altered by the addition of very low concentrations of $BaTiO_3$ or by the ultrasonication method used for solid particles reduction (Figure 4a), as expected. Furthermore, the thermogravimetric measurements showed that the weight loss of the elastomer modified with ceramic piezoelectric compound has the same decomposition behaviour than pristine NR (Figure 4b). The unique difference being found was for the char yield obtained at about 600ºC, which slightly increased from 0.3% to 1.3%, values being still low for polymer composites. All thermal data are showed on Table 2.

On the other hand, due to the better dispersion among solids and latex resin and, consequently, better elastomeric polymer obtaining, the mechanical properties slightly improved compared to the unmodified NR with similar film thickness (Table 2). The elongation at break has improved almost 15 ± 3~~.4~~% for the highest $BaTiO_3$ concentration (NR/$BaTiO_3$-0.50wt %), and about 20 ± 3% for the maximum tensile strength supported by the dumbbell specimens. All samples exhibited elastic fracture with no evidence of crevices or holes, as evidenced by SEM. The same tendency was found for the water contact angle measurements. The hydrophobicity of the films has been increased by 5-12% compared to the NR prepared without solids ultrasonication (Table 2). Therefore, the dispersion is the key for obtaining higher hidrophobic polymer composites and better performance.

SEM micrographs were taken, after freeze-fractured surface, for all films in order to observe the particle dispersions with increasing barium titanate concentration (Figure 5). Despite the cryo-fracture observed in all samples was elastic, films without solid additives sonication presented a large amount of amorphous phases distributed around elastic zones (white spots observed with InLens detector), as can be seen in the Figure 5a. On the other hand, these large white spots have almost been eliminated from the films with solid incorporation after sonication treatment (Figures 5b-e). The white particles seen in NR/$BaTiO_3$ composites upper cryo-fractured surfaces are solids from several kinds of additives instead of phase separation. The composite with better distribution ~~obtained~~ was NR/$BaTiO_3$-0.50wt % (Figure 5e), which has been also reflected on the dielectric results ~~obtained~~ (see next section discussion). Comparing the micrographs of the NR with 0.10 w% $BaTiO_3$ (Figure 5b) and 0.40 w% (Figure 5d), there was an important reduction of the amorphous phases separation compared to the pristine NR; while in the films with concentrations of 0.25 w% (Figure 5c) and 0.50 w% of $BaTiO_3$ (Figure 5e) it was not observed, indicating that all particles were well dispersed. Therefore, particle size influences the mechanical and electrical properties of the final product, reducing (more distinguishable amorphous phases) or increasing (less amorphous phase separations) the elastic behaviour of the crosslinked chains in the vulcanized rubber.

Dielectric properties of NR/$BaTiO_3$ solid films

The theory of electrical conduction in polymeric materials is extremely complex because the apparent current between electrodes separated by a polymeric material is neither constant in time nor proportional to the applied voltage. In this way, volume resistivity values for high insulating materials are usually in a wide range of over 10^{22} to 1 Ω·m [24]. While the volume resistivity (or rather volume conductivity) is a true measure of the charge transport through the bulk of the material, the surface resistivity is a measure of transport along the surface of the material. As the apparent ability of a material to conduct charge along its surface is extremely important in many applications, both parameters were evaluated in the present study. Surface (ρ_s) and volume (ρ_v) resistivity presented discrete variations, as shown in Table 3. There is a tendency of volume resistivity to increase with the increasing content of $BaTiO_3$. It is probably due to the high anisotropy obtained after rubber compounding. On the other hand, surface resistivity is one order of magnitude higher for

composites with high concentration of perovskite, for 5 min of DC voltage application. It can also be attributed to the better dispersion of solid particles and, therefore, reduction of solid aggregates upper surface. The DC electrical conductivity has been included in Table 3. The DC electrical conductivity ($\sigma_{dc,}$ S/cm) is the inverse of the volumetric resistivity (ρ_v, Ω·cm), according to the equation (1):

$$\sigma_{dc} = 1/\rho_v \qquad \text{Ec. (1)}$$

Some authors have been proved that the electrical conductivity in natural rubber samples is of ionic nature and has a tight dependence with temperature [25].

Moreover, impedance resistance varied a lot after barium titanate incorporation. As we can appreciate in ~~the~~ Figure 6, the Nyquist plot had only one semi-circle (one time constant), corresponding to highly capacitive samples for all NR modified with $BaTiO_3$ compared to the pristine rubber that presented more than one time constant (τ) (Figure 6a, inset). Usually, several time constants in a polymer film are related to more porous materials. The increased semi-circle impedance with increased content of $BaTiO_3$ nanoparticles reflects the better isolating properties of NR/$BaTiO_3$ thanks to the optimum dielectric properties offered by these ceramic additives and thanks to the low particle size achieved after sonication process. Electrical equivalent circuits (EEC) used for fitting experimental data are shown in the Figure 6b. As evidenced in the Table 4, the coating resistance increased for about one order of magnitude for NR/$BaTiO_3$-0.50wt.% (1.74×10^7 Ω·cm^2) compared to the sample without barium titanate (2.08×10^6 Ω·cm^2) after 24 hours in NaCl 3.5 wt.%. Pristine NR resulted in a more porous material with different interfaces denoted by three time constants appeared in the Nyquist plot (Figure 6a, inset), as mentioned before. Thus, EIS analysis demonstrated to be more effective to understand the electrical properties of highly insulating polymers by using AC conductivity than surface and volume resistivity measurements.

In the present study dielectric relaxation processes were also evaluated by EIS in the frequency range from 10 mHz to 1 MHz and at room temperature. The effective permittivity in polymeric nanocomposites is determined by dielectric polarisation in the bulk of the polymer film. Therefore, there will be polarisations associated to the rubber segments, to the synergistic effect among the oxide particles added to the rubber formulation and between the interfacial polarisations at the NR/particles interfaces. The prepared NR/$BaTiO_3$ has a large volume fraction of interfaces where the interfacial polarisations are most likely to occur.

The complex dielectric permittivity, breakdown strength, and conductivity (among other properties) are the primary interests for dielectric materials and are, in many cases, mutually dependent. Several works have reported the permittivity values for thermoplastic, thermostable and elastomer based polymers when insulating oxides are used as fillers [8,14-17,26-28], by using broadband impedance spectroscopy. In these works, the dielectric properties have been evaluated with increasing temperature, just to the dielectric sensitivity to temperature changes. In this work, only the AC dielectric response at room temperature was considered because the latex films are not intended to be used as high temperature dielectric material, *i.e.* we do not expect that the dielectric properties of NR films will change after the $BaTiO_3$ nanoparticle incorporation if it works below 120-130ºC (Curie temperature for $BaTiO_3$ piezoelectric material). Another important approach carried out in this work was the employment of NaCl aqueous solution as ionic conductive promoter in order to avoid the highly insulating permittivity limitation of our equipment.

The dielectric parameter as a function of frequency is described by the complex permittivity in the form:

$$\varepsilon^*(\omega) = \varepsilon'(\omega) - j\,\varepsilon''(\omega) \qquad \text{Eq. (2)}$$

where the real part $\varepsilon'(\omega)$ and imaginary part $\varepsilon''(\omega)$ are the components of the energy storage and energy loss, respectively, in each cycle of the electric field.

The measured capacitance (*C*, which is the CPE showed in Table 4) of the films was used to calculate the dielectric constant $\varepsilon'(\omega)$ using the following expression:

$$\varepsilon'(\omega) = \frac{C \cdot d}{A \cdot \varepsilon_0} \qquad \text{Ec. (3)}$$

where *d* is the film thickness, *A* is the surface area of sample,$\cdot\varepsilon_0$ is the permittivity of air (8.854×10^{-12} F·m^{-1}) and ω is the angular frequency.

Whereas, the imaginary part of the permittivity $\varepsilon''(\omega)$ is given by:

$$\varepsilon''(\omega) = \varepsilon'(\omega) \cdot \tan\delta(\omega) \qquad \text{Ec. (4)}$$

where $\tan\delta(\omega)$ is the dielectric loss tangent, which represents the relaxation parameter of the complexes numbers as a function of frequency.

In this study the obtained electric data from EIS analyses were first expressed in terms of real and imaginary part of dielectric permittivity and then transformed via equation (5) to the electric modulus presentation. Electric modulus is defined as the inverse quantity of complex permittivity:

$$M^*(\omega) = \frac{1}{\varepsilon^*(\omega)} = \frac{1}{\varepsilon' - j\varepsilon''} = \frac{\varepsilon'}{\varepsilon'^2+\varepsilon''^2} + j\frac{\varepsilon''}{\varepsilon'^2+\varepsilon''^2} = M' + jM'' \qquad \text{Ec. (5)}$$

where ε', M' and ε'', M'' are the real and imaginary parts of dielectric permittivity and electric modulus, respectively.

Thus, electrical relaxation phenomena present in composite polymers can be described via different formalisms, such as dielectric permittivity, electric modulus, AC conductivity, loss tangent, etc. However, electric modulus presentation has been proved suitable for neglecting the influence of electrode polarisation upon dielectric data, as described by Psarras and co-workers [27-30].

The variation of the real and imaginary part of dielectric permittivity as a function of frequency, at 25°C, for all samples are shown in Figures 7a and 7b. In all cases (ε' and ε'') diminish with frequency reflecting the decrease of polarisation, as expected. Nevertheless, despite the values at high frequencies are almost constant, detailed investigation reveals a decrease of permittivity with an increasing content of $BaTiO_3$ in all range. At 1000 Hz of frequency, the real permittivity of the highest content of perovskite has decreased more than twice the value of the pristine NR (Table 4) with the same film thickness. Values of the dielectric loss tangent (Figure 7c) varied from 2.83 to 0.96 for NR and NR/$BaTiO_3$-0.50 wt.%, respectively. Thus, with only 0.50 wt.% of $BaTiO_3$ it is possible to increase the insulating properties and improve the relaxation behaviour by 66% (tang δ) at 1000 Hz under AC current.

The tendency of decrease dielectric permittivity and dissipation factor is surprisingly different from other plastics, either thermoplastic, thermostable or elastomers [31], which always increase with filler content. Thanks to the very low concentration of $BaTiO_3$ inside rubber films, this unexpected behaviour should be explained by the synergistic combination of a non-polar polymer chain, with a homogenous amorphous phase distribution (as proved by SEM and DSC), and a very well wetted oxide fillers with nanometric particle size added by sonication. The smallest and superior filler distribution helped the polymer matrix to

decrease voids in the interface between particle and elastomer, increasing the storage energy of the composite material, and then decreasing the interfacial polarisation or the accumulation of charge in a local environment.

Analogous behaviour has been found for the electric modulus (Figures 7d and 7e), with a better relaxation phenomena of the interfacial polarisation observed at high frequencies than that obtained by dielectric permittivity. As can be seen, higher piezoelectric ceramic content implies a slight shift of the real and imaginary electric modulus to the left position. For example, in the Figure 7e, the interfacial polarisation predominate in the amorphous phase of sample NR/$BaTiO_3$-0.50 wt.% and it has a pronounced change at lower frequencies. It means that polymer matrix is becoming more amorphous and the polar nature of fillers has an influence in the non-polar nature of the NR.

Additionally, we can mention that the high values of dielectric parameters observed in Figure 7, compared to the dielectric permittivity or loss tangent of other hydrocarbons, are due to the presence of ionic conductivity molecules (from electrolyte used to swelling the sample before EIS analyses) inside the elastomer matrix. Nevertheless, it has not influence on the tendency explained by the relaxation behaviour of the composite dielectric elastomers, as the film thicknesses were well controlled.

Breakdown behaviour of NR/$BaTiO_3$ films

Testing for breakdown strength was performed according to the standard UNE-EN 60903, applying a frequency of 50Hz. Figure 8a shows a schematic representation of the breakdown test with the solid rubber specimens. Employing the experiment setup described before, the current versus voltage response was measured from 0 Volts up to breakdown conditions. Figure 8b represents the plot of voltage *versus* current until breakdown. Unfortunately, the addition of micron-sized fillers has often had a negative impact on breakdown strength [32]. This may be due to aggregation of filler particles, which are thought to introduce defect centres that distort and enhance the local electric field, resulting in reduced breakdown strength. It was observed in the composition without barium titanate in the Figure 8b, where the higher leakage current and lowest voltage breakdown values were obtained. This is the composition with the micron-sized fillers, as proved by SEM (Figure 5a). This field distortion is primarily due to the difference in the permittivity of the filler and the polymer

matrix under AC conditions. Also, as the particle size increases, the probability of field enhancement increases. However, when the fillers have nanometer dimensions, the filler-polymer interfacial area is large. Therefore, in the presence of a few weight percent of anisotropic fillers with high aspect ratio, the bulk polymer is converted into an interfacial polymer with favourable properties. Then, the NR sample with concentrations from 0.25 wt.% to 0.50 wt.% of $BaTiO_3$ nanoparticles and after solid sonication presented the lower leakage current and higher breakdown voltage compared to the pristine NR sample. Consequently, we have again proved that NR/$BaTiO_3$ composites have high ability to store energy and low polarizability at room temperature. The best electrically insulating elastomeric materials, which were able to store more energy until break were NR/$BaTiO_3$-0.25 wt.% and NR/$BaTiO_3$-0.40 wt.% with breakdown voltage of 24.8 kV/mm and 25.2 kV/mm and breakdown current of 0.72 mA/mm and 0.69 mA/mm, respectively. To conclude, better particle distribution and elimination of micro-voids were achieved with our method of combining fillers sonication and piezoelectric oxide compound addition, improving the breakdown strength of the rubbers.

4. CONCLUSIONS

Sonication-assisted mechanical mixing of $BaTiO_3$ nanoparticles (<100nm) inside the unvulcanized rubber helps the emulsion to be stable and avoid much amorphous phase separation after vulcanization process, as proved by SEM analyses. Addition of very low concentrations of $BaTiO_3$ was able to improve the electrical and mechanical properties of NR thin films.

The bulk resistance has also increased indicating that the composite films are highly insulating due to the decrease of the ionic conductivity in the polymer matrix.

NR composites with embedded ferroelectric ceramic nano-particles presented an unusual dielectric relaxation behaviour compared to common thermoplastic or thermostable polymers. Therefore, a decrease of permittivity and dissipation factor was found with increase $BaTiO_3$ content. Moreover, the amorphous phase has better insulating properties ~~and dielectric breakdown~~ when the nanoparticles are well dispersed as proved by the EIS and breakdown assays performed at room temperature.

For future perspective, the temperature dependence of the NR solid films should be tested with broadband impedance spectroscopy in order to check if the dielectric tendency

behaviour found for the natural elastomer will maintain in temperatures higher than the Curie temperature of $BaTiO_3$ piezoelectric filler.

Acknowledgements. The present work has been supported by Generalitat de Catalunya (Spain) with the Industrial Doctorate programme. N. González acknowledges the fellowship (2013DI036) promoted by the Industrial Doctorate programme.

REFERENCES

[1] A. Y. Coran, in *Handbook of Plastics Technologies.* Editor C. A. Harper, McGraw-Hill, New York, Chap. 4, 2006.

[2] J. L. White, *Rubber Processing Technology, Materials and Principles.* Hanser, New York, 1995.

[3] S. K. Srivastava, in Natural Rubber Materials, Volume 2: Composites and Nanocomposites. Eds. S. Thomas, H. J. Maria, J. Joy, C. H. Chan and L. A. Pothen. Royal Society of Chemistry, UK, Chap. 8, 2014.

[4] S. Salaeh, N. Muensit, P. Bomlai, C. Nakason, Ceramic/natural rubber composites: influence types of rubber and ceramic materials on curing, mechanical, morphological, and dielectric properties. J. Mater. Sci. 46 (2011) 1723–1731.

[5] Z-M. Dang, H-Y. Wang, Y-H. Zhang, J-Q. Qi, Morphology and Dielectric Property of Homogenous $BaTiO_3$/PVDF Nanocomposites Prepared via the Natural Adsorption Action of Nanosized $BaTiO_3$. Macrom. Rap. Comm. 26 (2005) 1185–1189.

[6] K. Yang, X. Huang, M. Zhu, L. Xie, T. Tanaka, P. Jiang. Combining RAFT Polymerization and Thiol-Ene Click Reaction for Core−Shell Structured Polymer@$BaTiO_3$ Nanodielectrics with High Dielectric Constant, Low Dielectric Loss, and High Energy Storage Capability. ACS Appl. Mat. Interf. 6 (2014) 1812–1822.

[7] S. Dalle Vacche, F. Oliveira, Y. Leterrier, V. Michaud, D. Damjanovic, J-A. E. Manson, The effect of processing conditions on the morphology, thermomechanical, dielectric, and piezoelectric properties of P(VDF-TrFE)/$BaTiO_3$ composites. J. Mat. Sci. 47 (2012) 4763–4774.

[8] S. Dalle Vacche, F. Oliveira, Y. Leterrier, V. Michaud, D. Damjanovic, J-A. E. Manson, Effect of silane coupling agent on the morphology, structure, and properties of poly(vinylidene fluoride–trifluoroethylene)/$BaTiO_3$ composites. J. Mat. Sci. 49 (2014) 4552–4564.

[9] L. Xie, X. Huang, B-W. Li, C. Zhi, T. Tanakae, P. Jiang, Core–satellite Ag@$BaTiO_3$ nanoassemblies for fabrication of polymer nanocomposites with high discharged energy density, high breakdown strength and low dielectric loss. Phys. Chem. Chem. Phys. 15 (2013) 17560–17569.

[10] C. R. Bowen, H. A. Kim, P. M. Weaver, S. Dunn, Piezoelectric and ferroelectric materials and structures for energy harvesting applications. Energy Environ. Sci. 7 (2014) 25–44.

[11] H. S. Jung, N-G Park, Perovskite Solar Cells: From Materials to Devices. Small 11 (2015) 10–25.

[12] C. G. Hardy, M. S. Islam, D. Gonzalez-Delozier, J. E. Morgan, B. Cash, B. C. Benicewicz, H. J. Ploehn, C. B. Tang, Converting an electrical insulator into a dielectric capacitor: end-capping polystyrene with oligoaniline, Chem. Mater. 25 (2013) 799–807.

[13] V. S. Puli, R. Elupula, B. C. Riggs, S. M. Grayson, R. S. Katiyar, D. B. Chrisey, Surface modified $BaTiO_3$-polystyrene nanocomposites for energy storage, Int. J. Nanotechnol. 11 (2014) 910–920.

[14] G. Ioannou, A. Patsidis, G.C. Psarras, Dielectric and functional properties of polymer matrix/ZnO/$BaTiO_3$ hybrid composites. Composites: Part A 42 (2011) 104–110.

[15] W. Yang, S.Yu, S. Luo, R. Sun, W-H. Liao, C-P. Wong. A systematic study on electrical properties of the BaTiO3-epoxy composite with different sized $BaTiO_3$ as fillers. J. Alloys Comp. 620 (2015) 315–323.

[16] Z-F. Zhang, X-F. Bai, J-W. Zha, W-K. Li, Z-M. Dang. Preparation and dielectric properties of BaTiO3/epoxy nanocomposites for embedded capacitor application. Compos. Sci. .Technol. 97 (2014) 100–105.

[17] S. Salaeh, G. Boiteux, P. Cassagnau, C. Nakason. Flexible 0-3 Ceramic-Polymer Composites of Barium Titanate and Epoxidized Natural Rubber. Int. J. Appl. Ceram. Technol. 12 (2015) 106–115.

[18] ASTM D257–07 An American National Standard Standard Test Methods for DC Resistance or Conductance of Insulating Materials.

[19] F. Müller, C. A. Ferreira, D. S. Azambuja, C. Alemán, E. Armelin, Measuring the Proton Conductivity of Ion-Exchange Membranes Using Electrochemical Impedance Spectroscopy and Through-Plane Cell, J. Phys. Chem. B 118 (2014) 1102–1112.

[20] IEC-60903 Live working – Electrical insulating gloves, ASTM D120–09 Standard Specification for Rubber Insulating Gloves.

[21] G. Liu, D. Zhang, T. W. Button, Preparation of concentrated barium titanate suspensions incorporating nano-sized powders. J. Eur. Ceram. Soc. 30 (2010) 171–176.

[22] S-J. Chang, W-S. Liao, C-J. Ciou, J-T. Lee, C-C. Li. An efficient approach to derive hydroxyl groups on the surface of barium titanate nanoparticles to improve its chemical modification ability. J. Coll. Interf. Sci. 329 (2009) 300–305.

[23] C-C. Li, S-J. Chang, J-T. Lee, W-S. Liao, Efficient hydroxylation of $BaTiO_3$ nanoparticles by using hydrogen peroxide. Coll. & Surf. A: Physicochem. Eng. Aspects 361 (2010) 143–149.

[24] C. Barry, in *Handbook of Polymer Testing. Physical Methods*. Editor R. Brown, Marcel Dekker Inc., New York, Chap. 25.

[25] A. Ladhar, M. Arous, H. Kaddami, M. Raihan, A. Kallel, M.P.F. Graça, L.C. Costa, AC and DC electrical conductivity in natural rubber/nanofibrillated cellulose nanocomposites, J. Molec. Liquids, 209 (2015), 272–279.

[26] S. Dalle Vacche, Y. Leterrier, V. Michaud, D. Damjanovic, A. B. Aebersold, J-A. E. Månson, Effect of interfacial interactions on the electromechanical response of poly(vinylidene fluoride-trifluoroethylene)/$BaTiO_3$ composites and its time dependence after poling. Comp. Sci. Techn. 114 (2015) 103–109.

[27] I. Asimakopoulos, L. Zoumpoulakis, G. C. Psarras. Development and characterization of novolac resin/$BaTiO_3$ nanoparticles composite system. J. Appl. Polym. Sci. 125 (2012) 3737–3744.

[28] I. A. Asimakopoulos , G. C. Psarras, L. Zoumpoulakis, Barium titanate/polyester resin nanocomposites: Development, structure-properties relationship and energy storage capability. Express Polym. Lett. 8 (2014) 692–707.

[29] A. Patsidis, G. C. Psarras. Dielectric behaviour and functionality of polymer matrix-ceramic $BaTiO_3$ composites. Express Polym. Lett. 2, (2008), 718–726.

[30] G. A. Kontos, A. L. Soulintzis, P. K. Karahaliou, G. C. Psarras, S. N. Georga, C. A. Krontiras, M. N. Pisanias. Electrical relaxation dynamics in TiO_2-polymer matrix composites. Express Polym. Lett. 1 (2007) 781–789.

[31] L. Jiang, A. Betts, D. Kennedy, S. Jerrams, Improving the electromechanical performance of dielectric elastomers using silicone rubber and dopamine coated barium titanate. Mater. Design 85 (2015) 733–742.

[32] Shen, Y.; Lin, Y.; Li, M.; Nan, C.W. High dielectric performance of polymer composite films induced by a percolating interparticle barrier layer. Adv. Mater. 19 (2007) 1418–1422.

Table 1. Compounding formulation used to prepare NR/ $BaTiO_3$ composites (in % phr)[a].

Reagents	NR	$BaTiO_3$ 0.10 wt%	$BaTiO_3$ 0.25 wt%	$BaTiO_3$ 0.40 wt%	$BaTiO_3$ 0.50 wt%
NR	100	100	100	100	100
Acelerator	6.0	6.0	6.0	6.0	6.0
Sulfur	6.0	6.0	6.0	6.0	6.0
Antioxidant	8.0	8.0	8.0	8.0	8.0
ZnO	8.0	8.0	8.0	8.0	8.0
TiO_2	5.0	4.0	2.5	1.0	-
$BaTiO_3$	-	1.0	2.5	4.0	5.0
Other fillers	7.0	7.0	7.0	7.0	7.0

[a] phr = parts per hundred parts of rubber, by mass.

Table 2. Thermal, mechanical and hydrophobicity properties for rubber films modified with $BaTiO_3$ nanoparticles.

Sample	T_g [a] (ºC)	$T_{d,max}$ [b] (ºC)	Char yield (%)	σ_{max} [c] (MPa)	σ_r [d] (MPa)	ε [e] (%)	WCA [f] (°)	Thickness (mm)
NR	-63	375	0.3	3.0 ± 0.1	22.4 ± 0.5	720 ± 29	110 ± 1	1.002
NR/$BaTiO_3$-0.10 wt%	-63	376	1.3	3.9 ± 0.1	24.0 ± 1.5	887± 34	116 ± 2	1.084
NR/$BaTiO_3$-0.25 wt%	-62	377	1.3	4.5 ± 0.3	23.7 ± 1.1	913 ± 31	119 ± 2	1.167
NR/$BaTiO_3$-0.40 wt%	-63	378	1.5	3.7 ± 0.1	23.3 ± 2.7	897 ± 32	123 ± 1	1.095
NR/$BaTiO_3$-0.50 wt%	-63	378	1.6	3.6 ± 0.1	27.4 ± 2.3	822 ± 24	121 ± 1	1.088

[a] Glass transition temperature obtained by DSC in the second scan after dynamic curing at 20ºC/min, [b] Temperature of the maximum decomposition rate based on the TGA data at 10ºC/min, [c] Maximum tensile strength, [d] Tensile strength at break, [e] Maximum elongation at break after 5 stress-strain measurements, [f] Water contact angle average after 10 measurements of static water droplet.

Table 3. Surface resistivity (σ_s), volume resistivity (ρ_v) and DC conductivities (σ) of NR films modified with $BaTiO_3$ nanoparticles.

Sample	ρ_v ($10^{16}\Omega$.cm) 1 min	ρ_v ($10^{16}\Omega$.cm) 5 min	σ_{dc} (10^{-16}S/cm) 1 min	σ_{dc} (10^{-16}S/cm) 5 min	ρ_s ($10^{15}\Omega$) 1 min	ρ_s ($10^{16}\Omega$) 5 min	Thickness (mm)
NR	0.12 ± 0.01	0.26 ± 0.01	8.33 ± 0.01	3.85×10^{-16}	0.20 ± 0.01	0.43 ± 0.01	0.912
NR/$BaTiO_3$-0.10 wt%	1.11 ± 0.03	1.83 ± 0.01	0.90 ± 0.03	0.55×10^{-16}	1.88 ± 0.01	0.53 ± 0.03	0.968
NR/$BaTiO_3$-0.25 wt%	1.21 ± 0.01	2.11 ± 0.13	0.83 ± 0.01	0.47×10^{-16}	3.97 ± 0.10	1.09 ± 0.01	0.991
NR/$BaTiO_3$-0.40 wt%	1.48 ± 0.01	2.90 ± 0.21	0.68 ± 0.01	0.34×10^{-16}	5.70 ± 0.12	3.60 ± 0.10	0.957
NR/$BaTiO_3$-0.50 wt%	0.15 ± 0.01	0.34 ± 0.01	6.67 ± 0.01	2.94×10^{-16}	4.65 ± 0.01	7.32 ± 0.01	1.053

Table 4. Coating resistance (R_c), constant phase elements (CPE) and dielectric parameters (at 1000 Hz and room temperature) for each sample analysed with a capacitor cell and after adjusting the parameters using the electrical equivalent circuit (EEC) shown in Figure 6b.

Sample	R_c ($\Omega.cm^2$)	CPE_c ($F\ cm^{-2}\ s^{n-1}$)	n	ε' 1000 Hz	ε'' 1000 Hz	tanδ 1000 Hz	Thickness (mm)
NR	2.08×10^6	2.22×10^{-10}	0.75	13.78	39.02	2.83	0.710
NR/$BaTiO_3$-0.10 wt%	2.49×10^6	6.80×10^{-11}	0.83	8.89	29.34	3.30	0.711
NR/$BaTiO_3$-0.25 wt%	9.91×10^6	2.21×10^{-10}	0.74	9.89	11.78	1.19	0.749
NR/$BaTiO_3$-0.40 wt%	6.71×10^6	2.30×10^{-10}	0.73	10.50	15.67	1.49	0.717
NR/$BaTiO_3$-0.50 wt%	1.74×10^7	8.46×10^{-11}	0.79	6.00	5.80	0.96	0.708

FIGURE CAPTIONS

Figure 1. SEM micrographs from $BaTiO_3$ nanoparticles in an oil emulsion (a), detail of agglomerates inside a droplet (b) and micrograph of rubber film surface showing the main agglomerates identified as $BaTiO_3$ (c). Inset in (b) indicates a part of drop oil cut where picture has been taken and arrows in (c) indicate the specific zones where $BaTiO_3$ agglomerates have been detected by EDX.

Figure 2. SEM micrographs of $BaTiO_3$ solid particles before (a) and from solid film surface (b), after compounding. EDX composition of $BaTiO_3$ nanoparticles inside rubber solid film (c).

Figure 3. Infrared spectrum with the absorption bands comparison between the films prepared without sonicated solids and after particle size decreasing by sonication and after addition of $BaTiO_3$ nanoparticles.

Figure 4. (a) DSC thermograms of the second scan after dynamic curing at 20ºC/min and (b) thermogravimetric curves at 10 ºC/min in N_2 atmosphere for NR vulcanized films. The inset on (b) represents the char yield at 600ºC.

Figure 5. Cross-sectional SEM micrographs taken at low (left), medium (centre) and high (right) magnifications of (a) NR as-prepared, *i.e.* without solid particles size reduction; NR modified with $BaTiO_3$ and after sonication of solid additives: (b) 0.10 wt. %, (c) 0.25 wt. %, (d) 0.40 wt. %, and (e) 0.50 wt. %.

Figure 6. (a) Nyquist plots for pristine NR and NR modified with different concentrations of barium titanate and (b) electrical equivalent circuit (EEC) used for fitting experimental data: NR/$BaTiO_3$-0.10 wt%, NR/$BaTiO_3$-0.25 wt%, NR/$BaTiO_3$-0.50 wt% (upper) and pristine NR, NR/$BaTiO_3$-0.40 wt% (down). The inset in (a) corresponds to the magnification of NR plot and dashed lines represent the curves from fitting data.

Figure 7. (a) Real dielectric permittivity, (b) imaginary dielectric permittivity, (c) dielectric loss tangent, (d) real electric modulus and (e) imaginary electric modulus as a function of frequency for several weight percentage of $BaTiO_3$ nanoparticles.

Figure 8. (a) Schematic representation of the breakdown test applied in a ~~real latex glove~~ latex specimen, where D represents the height of sample that must be outside water; and (b) AC polarisation curves obtained from breakdown strength measurements for solid rubber specimens showed in the Scheme 1, obtained after vulcanization in a mould from glass tubes. All samples were controlled to be 1.0 mm of thickness and 15 mm of diameter.

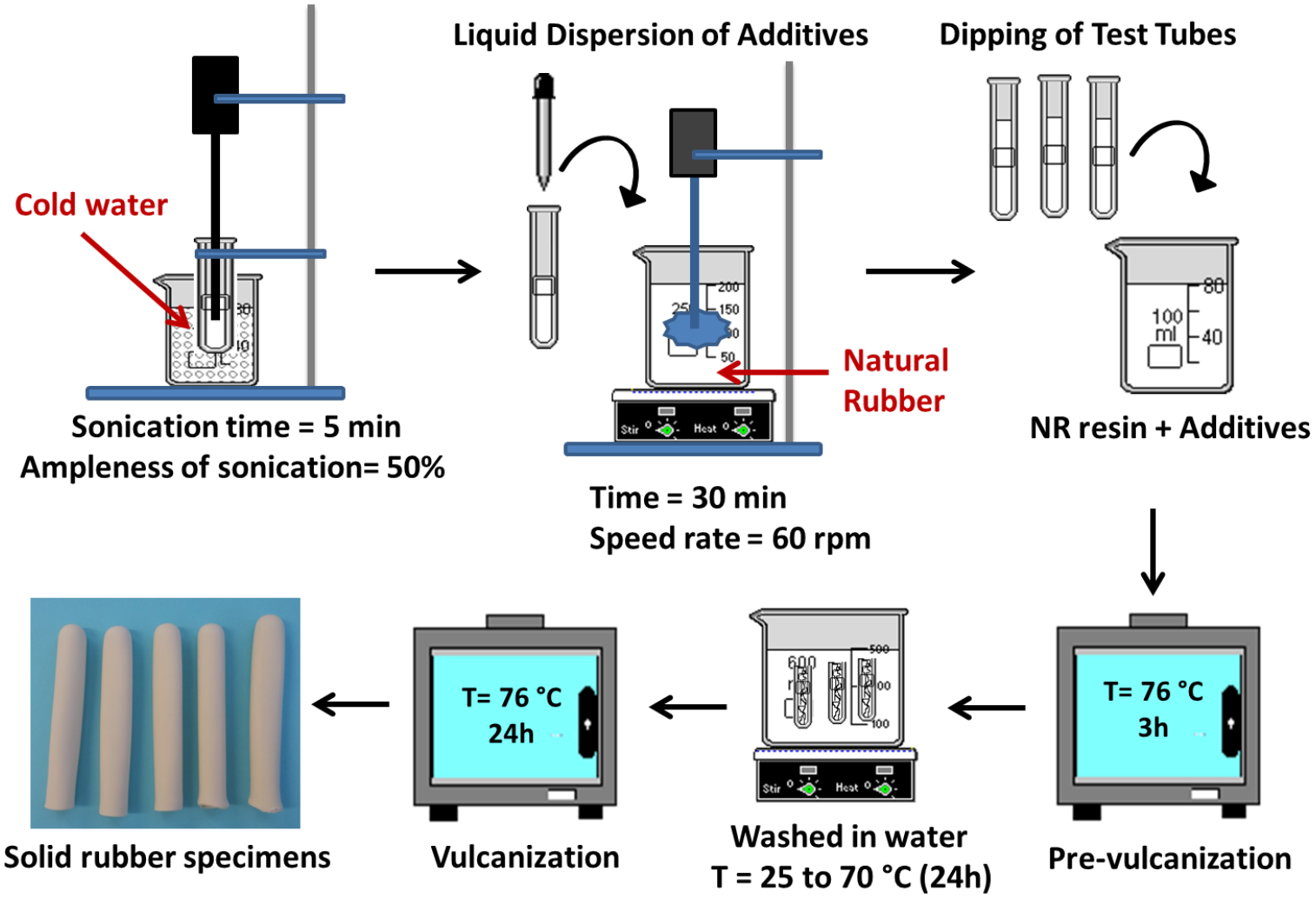
Cold water
Sonication time = 5 min
Ampleness of sonication= 50%
Liquid Dispersion of Additives
Natural Rubber
Time = 30 min
Speed rate = 60 rpm
Dipping of Test Tubes
NR resin + Additives
T= 76 °C
3h
Pre-vulcanization
Washed in water
T = 25 to 70 °C (24h)
T= 76 °C
24h
Vulcanization
Solid rubber specimens

Scheme 1

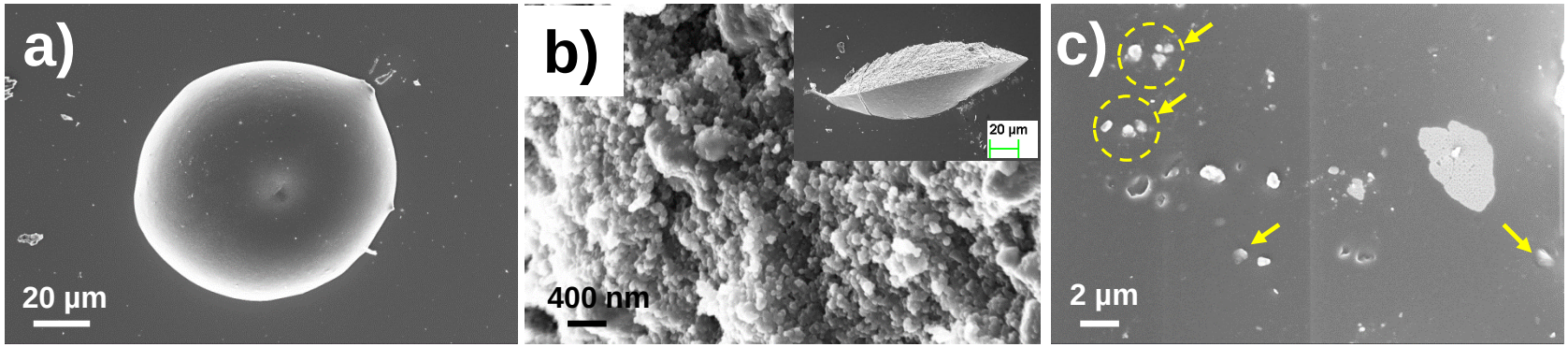

Figure 1

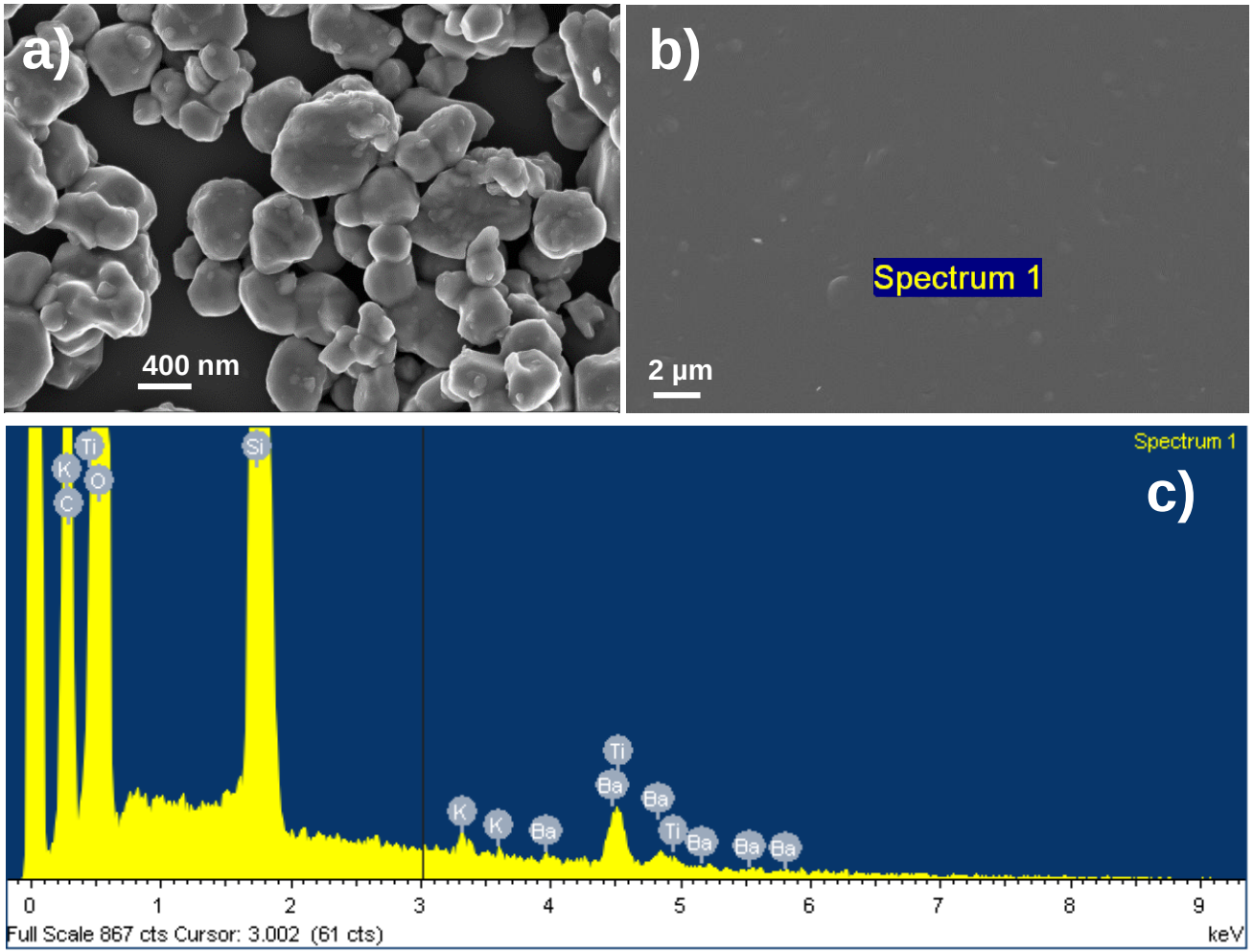
a)
400 nm
b)
Spectrum 1
2 µm
Spectrum 1
c)
Ti
K
O
C
Si
K
K
Ba
Ti
Ba
Ba
Ti
Ba
Ba
Ba
0
1
2
3
4
5
6
7
8
9
Full Scale 867 cts Cursor: 3.002 (61 cts)
keV

Figure 2

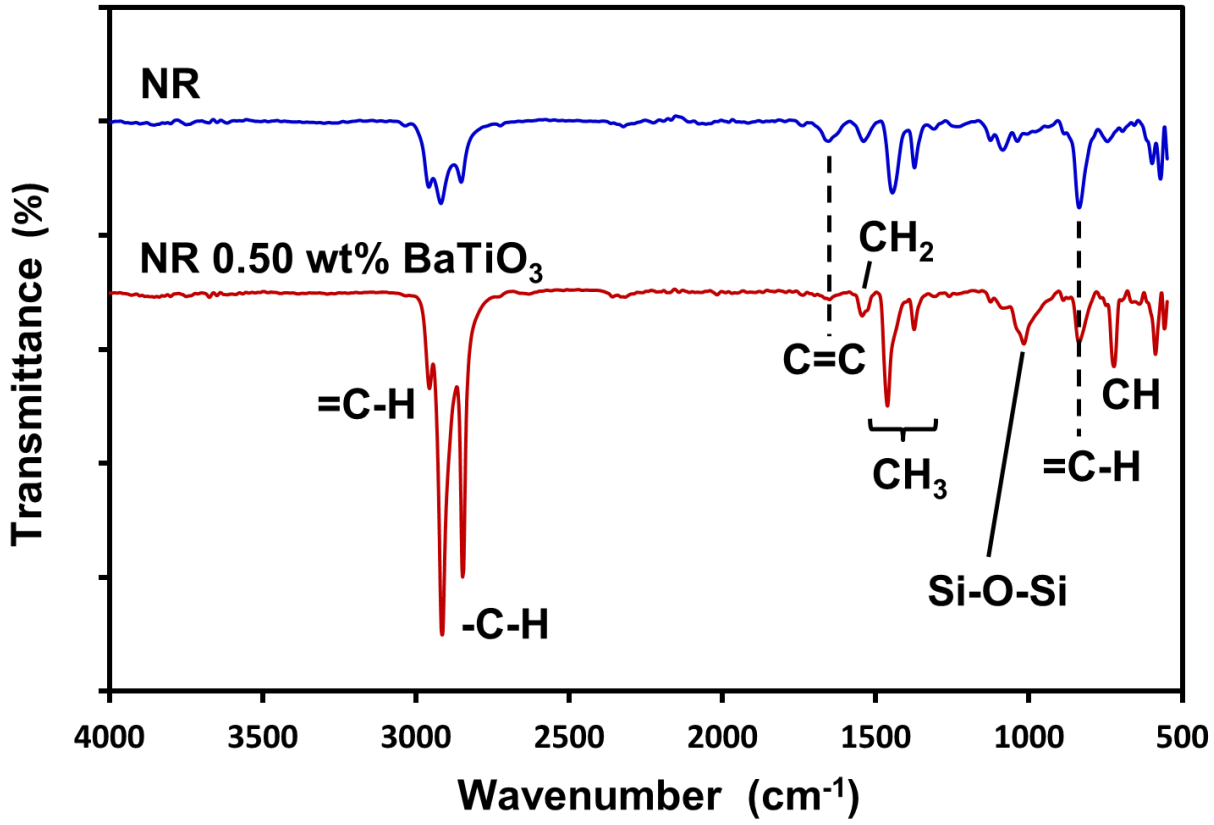
NR
NR 0.50 wt% BaTiO3
Transmittance (%)
CH2
C=C
CH
CH3
=C-H
=C-H
Si-O-Si
-C-H
4000
3500
3000
2500
2000
1500
1000
500
Wavenumber (cm-1)

Figure 3

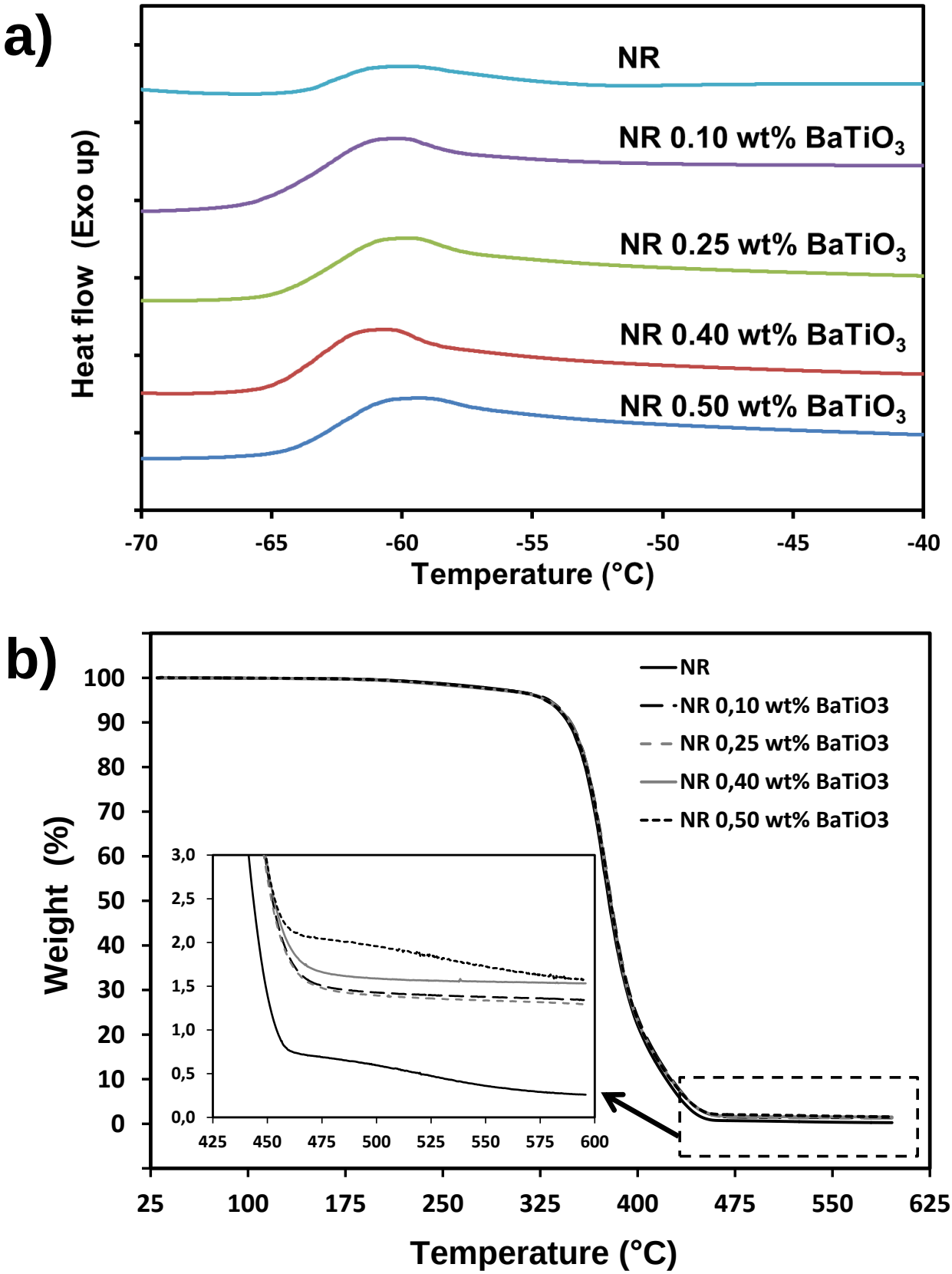
a)
NR
NR 0.10 wt% BaTiO3
NR 0.25 wt% BaTiO3
NR 0.40 wt% BaTiO3
NR 0.50 wt% BaTiO3
Heat flow (Exo up)
-70
-65
-60
-55
-50
-45
-40
Temperature (°C)
b)
NR
NR 0,10 wt% BaTiO3
NR 0,25 wt% BaTiO3
NR 0,40 wt% BaTiO3
NR 0,50 wt% BaTiO3
Weight (%)
100
90
80
70
60
50
40
30
20
10
0
3,0
2,5
2,0
1,5
1,0
0,5
0,0
425
450
475
500
525
550
575
600
25
100
175
250
325
400
475
550
625
Temperature (°C)

Figure 4

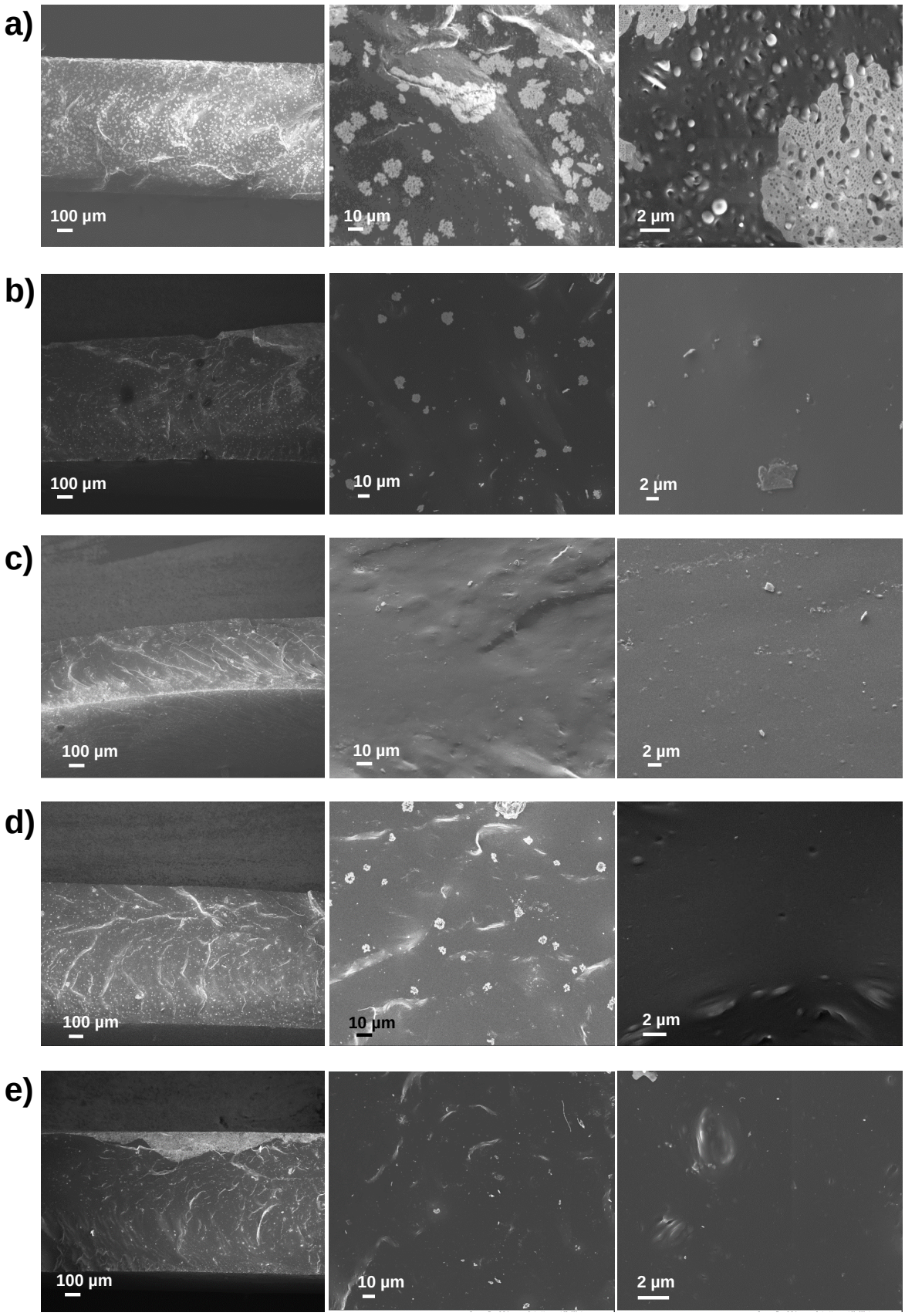
a)
100 µm
10 µm
2 µm
b)
100 µm
10 µm
2 µm
c)
100 µm
10 µm
2 µm
d)
100 µm
10 µm
2 µm
e)
100 µm
10 µm
2 µm

Figure 5

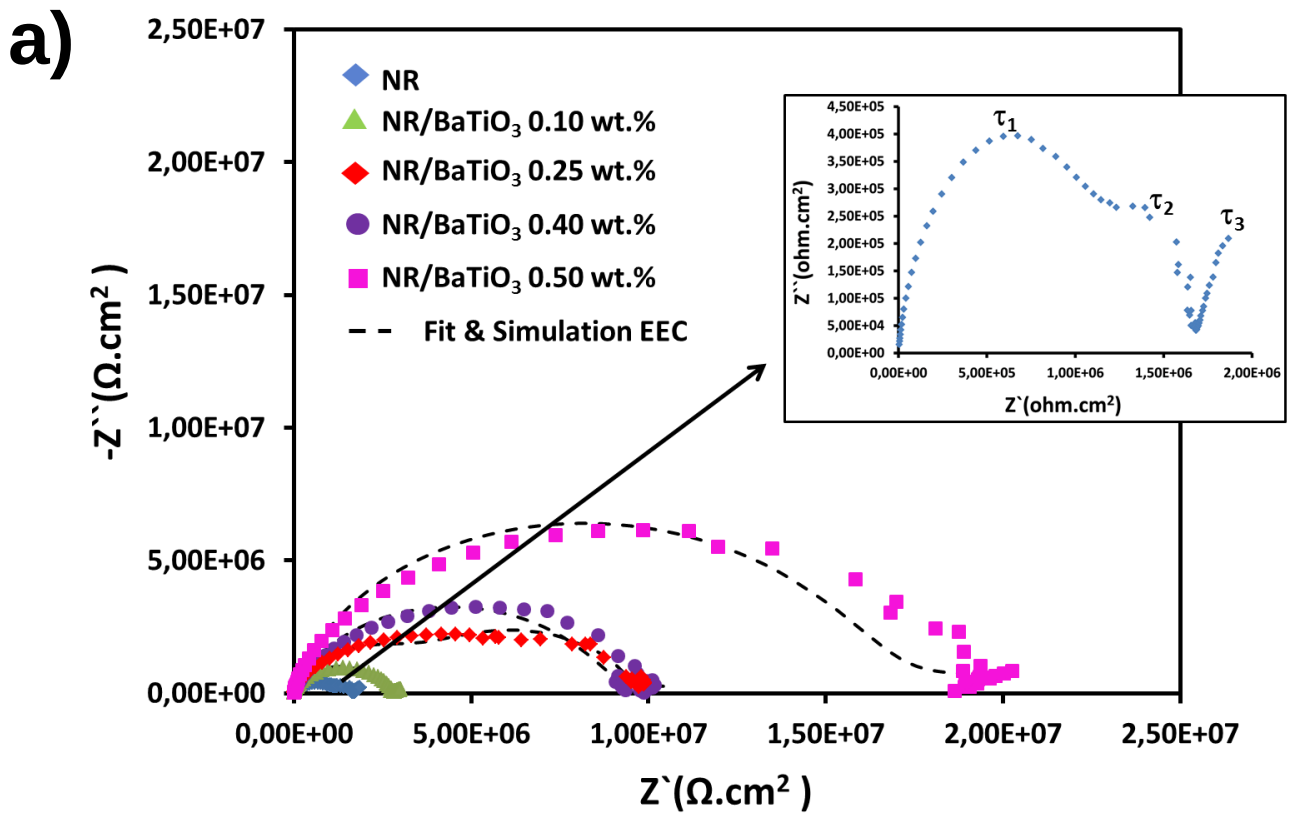
a)
NR
NR/BaTiO3 0.10 wt.%
NR/BaTiO3 0.25 wt.%
NR/BaTiO3 0.40 wt.%
NR/BaTiO3 0.50 wt.%
Fit & Simulation EEC
-Z``(Ω.cm2)
Z`(Ω.cm2)
2,50E+07
2,00E+07
1,50E+07
1,00E+07
5,00E+06
0,00E+00
0,00E+00
5,00E+06
1,00E+07
1,50E+07
2,00E+07
2,50E+07
τ1
τ2
τ3
Z``(ohm.cm2)
Z`(ohm.cm2)
4,50E+05
4,00E+05
3,50E+05
3,00E+05
2,50E+05
2,00E+05
1,50E+05
1,00E+05
5,00E+04
0,00E+00
0,00E+00
5,00E+05
1,00E+06
1,50E+06
2,00E+06

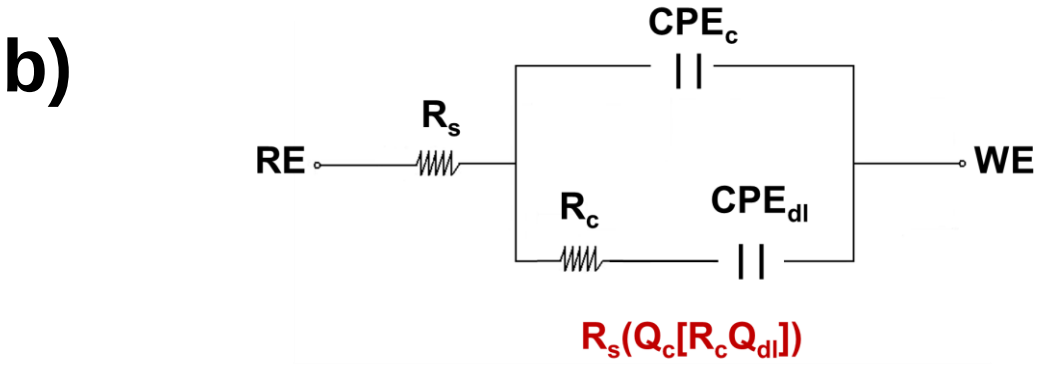
b)
CPEc
Rs
RE
WE
Rc
CPEdl
Rs(Qc[RcQdl])

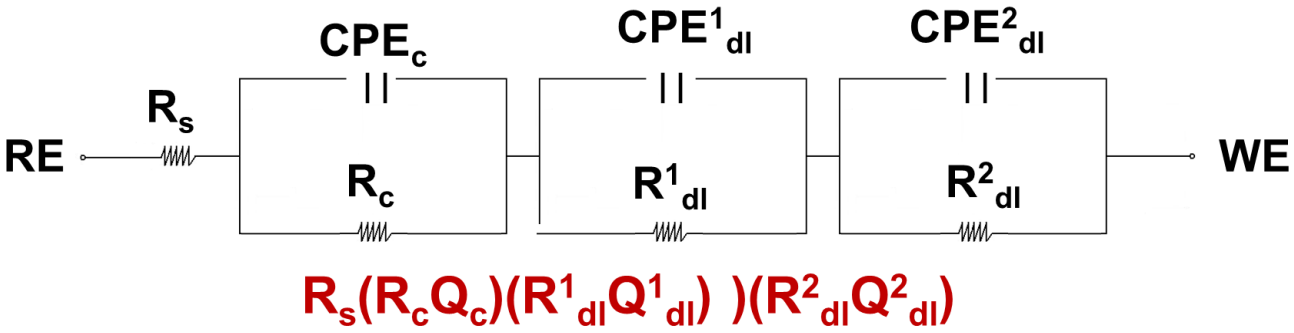
CPEc
CPE1dl
CPE2dl
Rs
RE
WE
Rc
R1dl
R2dl
Rs(RcQc)(R1dlQ1dl))(R2dlQ2dl)

Figure 6

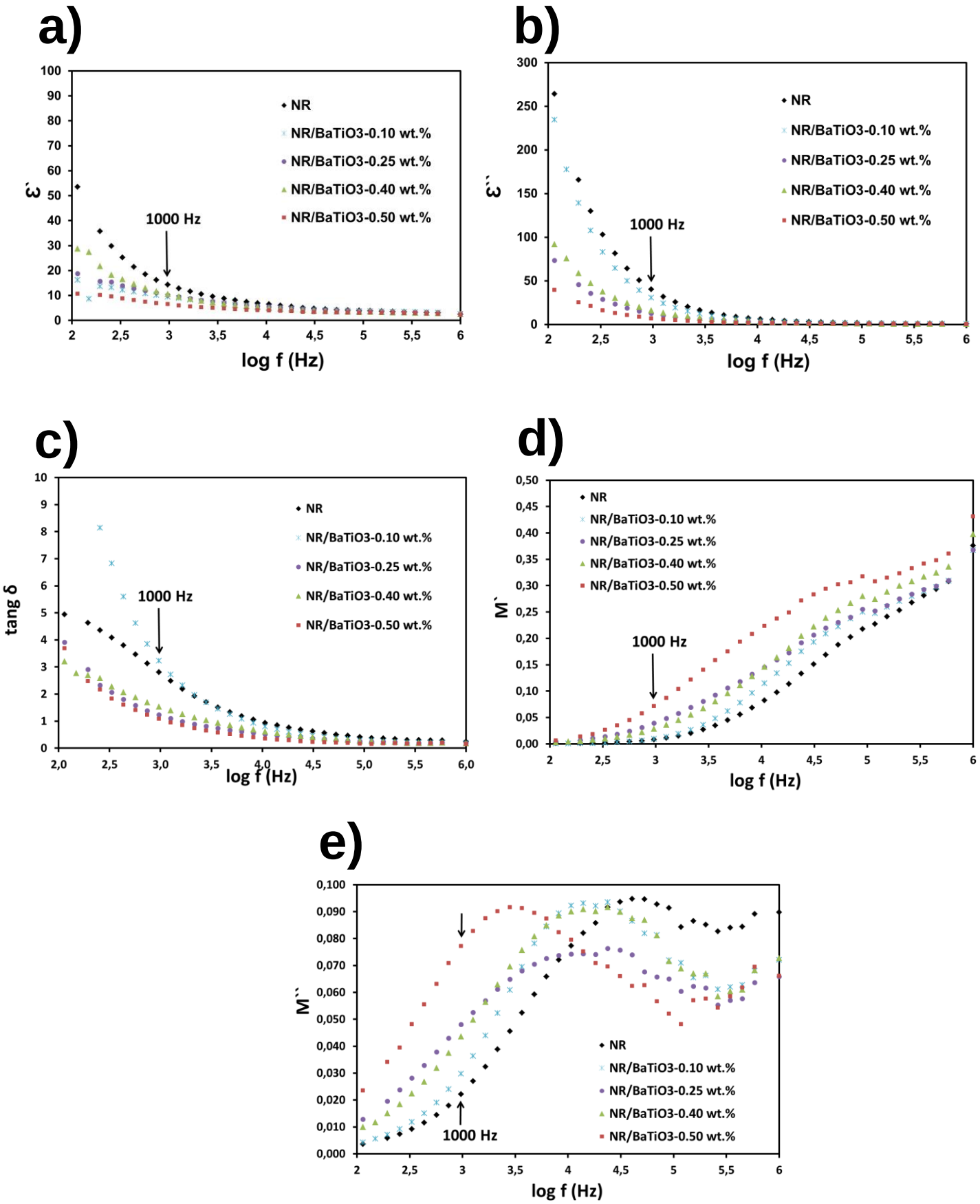
a)
ε`
log f (Hz)
1000 Hz
NR
NR/BaTiO3-0.10 wt.%
NR/BaTiO3-0.25 wt.%
NR/BaTiO3-0.40 wt.%
NR/BaTiO3-0.50 wt.%
b)
ε``
log f (Hz)
1000 Hz
c)
tang δ
log f (Hz)
d)
M`
log f (Hz)
e)
M``
log f (Hz)

Figure 7

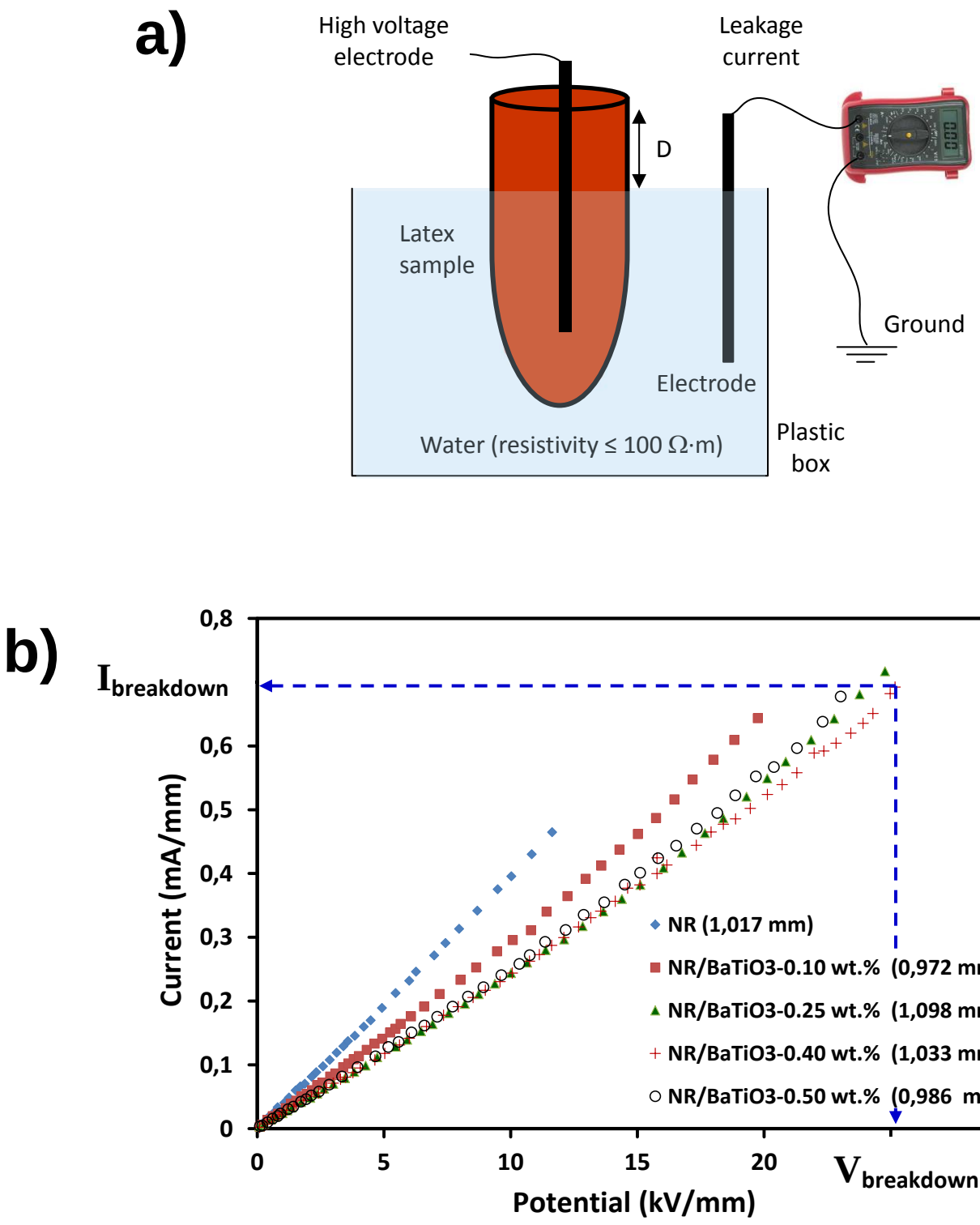
a)
High voltage electrode
Leakage current
D
Latex sample
Ground
Electrode
Water (resistivity ≤ 100 Ω·m)
Plastic box
b)
$I_{breakdown}$
Current (mA/mm)
Potential (kV/mm)
$V_{breakdown}$
0,8
0,6
0,5
0,4
0,3
0,2
0,1
0
0
5
10
15
20
30
NR (1,017 mm)
NR/BaTiO3-0.10 wt.% (0,972 mm)
NR/BaTiO3-0.25 wt.% (1,098 mm)
NR/BaTiO3-0.40 wt.% (1,033 mm)
NR/BaTiO3-0.50 wt.% (0,986 mm)

Figure 8